Severe acute respiratory syndrome-associated coronavirus 3a protein forms an ion channel and modulates virus release

Wei Lu*†‡§, Bo-Jian Zheng§¶, Ke Xu*†, Wolfgang Schwarz‡‖, Lanying Du¶, Charlotte K. L. Wong¶, Jiadong Chen, Shuming Duan**, Vincent Deubel*, and Bing Sun*†,††**

*Laboratory of Molecular Virology, Institut Pasteur of Shanghai, Chinese Academy of Sciences, 225 South Chongqing Road, Shanghai 200025, China; †Laboratory of Molecular Cell Biology, Institute of Biochemistry and Cell Biology, ‡Max Planck Guest Laboratory, and **Shanghai Institute of Neuroscience, Shanghai Institute of Biological Sciences, Chinese Academy of Sciences, 320 Yueyang Road, Shanghai 200031, China; ¶Department of Microbiology, University of Hong Kong and Queen Mary Hospital, Hong Kong, China; and ‖Max Planck Institute for Biophysics, Max-von-Laue-Strasse 3, 60438 Frankfurt/M, Germany

Communicated by Zhu Chen, Shanghai Second Medical University, Shanghai, China, June 30, 2006 (received for review June 22, 2006)

Fourteen ORFs have been identified in the severe acute respiratory syndrome-associated coronavirus (SARS-CoV) genome. ORF 3a of SARS-CoV codes for a recently identified transmembrane protein, but its function remains unknown. In this study we confirmed the 3a protein expression and investigated its localization at the surface of SARS-CoV-infected or 3a-cDNA-transfected cells. Our experiments showed that recombinant 3a protein can form a homotetramer complex through interprotein disulfide bridges in 3a-cDNA-transfected cells, providing a clue to ion channel function. The putative ion channel activity of this protein was assessed in 3a-complement RNA-injected *Xenopus* oocytes by two-electrode voltage clamp. The results suggest that 3a protein forms a potassium sensitive channel, which can be efficiently inhibited by barium. After FRhK-4 cells were transfected with an siRNA, which is known to suppress 3a expression, followed by infection with SARS-CoV, the released virus was significantly decreased, whereas the replication of the virus in the infected cells was not changed. Our observation suggests that SARS-CoV ORF 3a functions as an ion channel that may promote virus release. This finding will help to explain the highly pathogenic nature of SARS-CoV and to develop new strategies for treatment of SARS infection.

ORF 3a | two-electrode voltage clamp | tetramer | channel activity

Outbreak of severe acute respiratory syndrome (SARS) in 2002 caused alarm all over the world. The newly discovered human coronavirus named SARS-associated coronavirus (SARS-CoV) was identified as the causative agent for this disease (1, 2). SARS-CoV has a large single-positive-strand RNA genome that contains 14 ORFs. Some of these ORFs encode viral structural proteins, such as spike protein, membrane protein, small envelope protein, and nucleocapsid protein, as well as viral replicase and protease (3). Those proteins play important roles in viral infection and replication. However, functions for other ORFs are not clear. Therefore, identification and characterization of new functional proteins from the ORFs will be helpful for understanding the pathogenesis of SARS-CoV. Up to now there are still no effective drugs or vaccines against SARS-CoV. The identification of new viral proteins and the elucidation of their functions will provide potential targets for design of drugs or vaccines against SARS.

Our previous work has revealed that ORF 3a of SARS-CoV is such a viral protein (4). Since then, other publications have concurred in this observation and have shown that it is a structural protein (5–8). ORF 3a is located between the S and E protein loci and encodes a protein of 274 aa. The only available information based on proteomics and immunoblotting suggests that 3a protein is structural in nature, but its localization, topology, and biological function have not been identified.

A computed biology analysis of the amino acid sequence of the 3a protein revealed that it has low similarity with any other known protein. Its C-terminal region shares ≈50% similarity to *Plasmodium* calcium pump protein and to the *Shewanella* outer-membrane porin. Interestingly, comparison of ORFs between S and E loci from different human coronaviruses (HCoV-2291 and HCoV-OC43) showed that SARS-CoV ORF encodes only the full-length 3a protein, and that other 3a proteins were truncated at their C termini (4). Based on this study, we assumed that the function of 3a protein may be involved in the acute pathogenesis of SARS-CoV and lethality in SARS patients.

In our present study, we analyzed the structural and biochemical features of 3a protein and found that 3a forms an ion channel in *Xenopus* oocytes. In addition, reduction of 3a protein expression in FRhK-4 cells with siRNA, when infected with SARS-CoV, significantly decreased SARS virus release. Our observations indicate that 3a protein is a functional membrane protein regulating virus release.

Results

Confirmation of 3a Protein Expression in SARS-CoV Infection. Initially, to confirm whether 3a protein was expressed in SARS patients and was immunogenic, IgG antibodies against a 3a protein-related antigenic epitope (LH21 peptide) were measured by ELISA in sera of 13 SARS patients and 13 healthy individuals. Results show that SARS patients' sera contain high levels of IgG recognizing 3a protein (Fig. 1*A*).

To test the specificity of LH21-specific polyclonal antibody (Ab), protein 3a expression in virus-infected FRhK-4 cells was studied by Western blot assay. A 37-kDa protein (3a protein) was recognized by the anti-LH21 Ab in virus-infected cell lysate but not in uninfected cell lysate (Fig. 1*B*), which indicates an active expression of 3a protein in the virus-infected cells. To determine the location of 3a protein in virus-infected cells, 3a protein distribution in FRhK-4 cells was analyzed by confocal microscopy. Fig. 1*C* reveals a high density of the 3a protein at the cell membrane and also in the cytoplasm and the nucleus of the infected cells. The observation of 3a protein on the cell surface of SARS-CoV-infected cells deserved further investigation.

3a Protein Is Located at the Cell Surface. To study the orientation of 3a protein on the cell surface, FRhK-4 cells were transfected with 3a recombinant plasmid in which the HA tag was linked to 3a protein at the C terminus. The orientation of 3a protein was analyzed by using 3a-specific Ab (anti-LH21) at the N terminus and

Conflict of interest statement: No conflicts declared.

Abbreviations: cRNA, complement RNA; SARS, severe acute respiratory syndrome; SARS-CoV, SARS-associated coronavirus.

§W.L. and B.-J.Z. contributed equally to this work.

††To whom correspondence should be sent at the * address. E-mail: bsun@sibs.ac.cn.

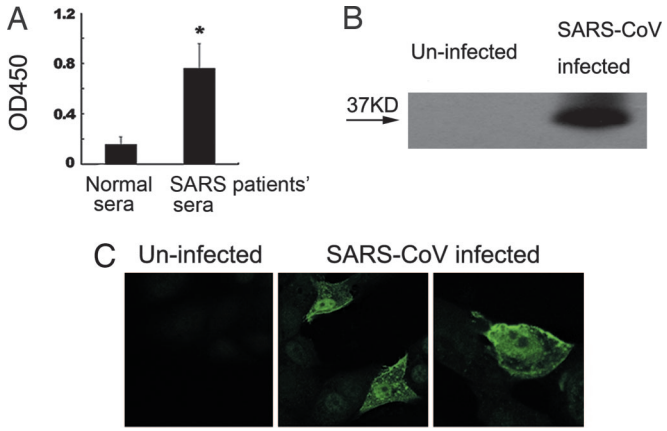

Fig. 1. 3a protein presence *in vivo* and *in vitro*. (*A*) Serological assay for detecting specific IgG Abs against 3a protein in sera from SARS patients ($n = 13$) and healthy controls ($n = 13$) by ELISA (*, $P < 0.01$). Virus-infected FRhK-4 cells were used for Western blot (*B*) and confocal microscopy assay (*C*). Anti-LH21 Ab was used in both Western blot and confocal microscopy assays.

anti-HA Ab at the C terminus (Fig. 2*A*). After permeabilization of the transfected cells, 3a protein was detected by both anti-LH21 and anti-HA Abs, and it was located at the cell membrane and in the cytoplasm. In contrast, in nonpermeabilized cells the 3a protein can be detected only by anti-LH21 at the cell membrane (Fig. 2*B*). These findings demonstrate that 3a protein is a transmembrane protein with an extracellular N terminus and an intracellular C terminus (Fig. 2*C*). Our finding, similar to former report (9), defines a rough topology of 3a protein on the cell membrane.

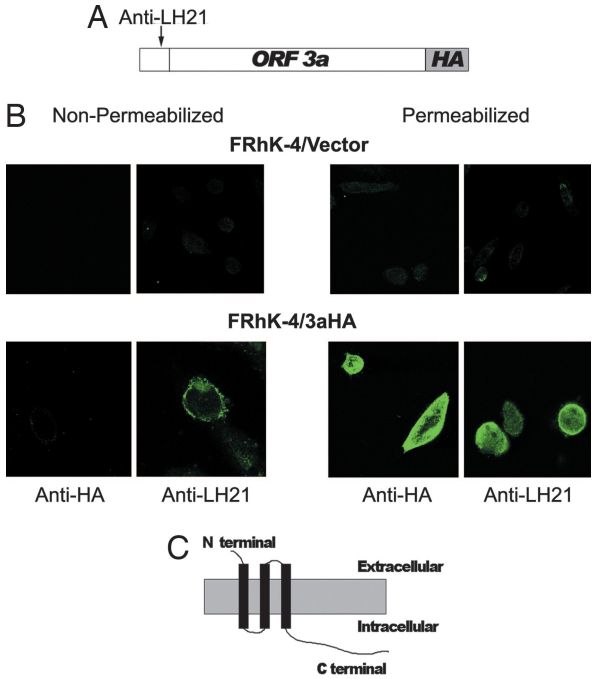

Fig. 2. Orientation of the 3a protein on the cell membrane. (*A*) Two specific antibodies were used for 3a protein orientation analysis. Anti-LH21 was directed against the N terminus of 3a protein, whereas anti-HA Ab was directed against the HA tag linked to the C terminus of 3a protein. (*B*) 3a- and vector-transfected FRhK-4 cells were permeabilized or nonpermeabilized, and 3a protein expressed on the cell surface was immunolabeled with anti-LH21 and anti-HA Abs, respectively. (*C*) An orientation model of the 3a protein at the cell surface. The extracellular N terminus, the intracellular C terminus, and the transmembrane domains are depicted in the model.

3a Protein Forms Homotetramers. In preliminary experiments using Western blotting with anti-LH21 Ab, we observed monomeric (37 kDa) and larger protein complexes of 3a protein in SARS-CoV-infected cell lysates and in 3a plasmid-transfected cell lysates (data not shown). To assess whether these complexes were aggregates or an oligomeric form of 3a protein, biosynthesis of 3a protein fused to HA tag was studied in transfected HEK293 cells. After 24–36 h, 3a proteins were immunoprecipitated by using anti-HA monoclonal Ab and then analyzed by Western blot with anti-LH21 Ab. In addition to the band corresponding to monomeric 3a protein (37 kDa), two other bands of ≈75 kDa and 150 kDa were observed (Fig. 3*A Left*). To assess whether these two additional bands corresponded to homodimers and homotetramers of the 3a protein, immunoprecipitates were treated with DTT before SDS/PAGE. After treatment with DTT, the bands of 75 kDa and 150 kDa disappeared (Fig. 3*A Right*). The sizes of 75 kDa and 150 kDa destroyed by DTT strongly suggest that they may correspond to homodimers and homotetramers of 3a protein.

A cysteine-rich domain can be found in the 3a protein sequence (4), which is located at amino acid residues 81–160 (Fig. 3*B*). To investigate which of the eight disulfide bonds in this domain are involved in the 3a protein polymerization, eight point mutations were introduced in the 3a gene in which each cysteine was replaced by alanine. Immunoprecipitates of HEK293 cells transfected by each of the recombinant mutated 3a genes were tested by SDS/PAGE and Western blot without DTT treatment. Fig. 3*C* shows that only the M6 mutation modified the capacity of 3a protein to polymerize. However, mutation M6 on cysteine 133 led to near abrogation of both dimers and tetramers of the protein, suggesting that this cysteine is involved in 3a protein polymerization. Based on this result, we assumed that 3a protein itself was linked by cysteine-133 to form a homodimer and that the homotetramer was made up of two dimers held together by noncovalent interactions.

To confirm that the 75-kDa and 150-kDa complexes are dimers and tetramers constituted by 3a proteins only, FRET was used (10, 11). 3aCFP and 3aYFP recombinant plasmids were constructed and used to transfect HeLa cells. M6CFP and M6YFP plasmids were also tested. Plasmid with inserted YFP–CFP fusion protein gene was used as a positive control. The relevant region of interest was analyzed, and the increase in CFP intensity, indicating FRET, was plotted against the decrease of YFP intensity. For the 3aCFP and 3aYFP group FRET efficiency was detected ($21.3 + 3.6\%$; $n = 10$). The results demonstrated that 3aCFP and 3aYFP proteins can be tightly linked together, forming the protein complex. M6CFP and M6YFP proteins exhibited a FRET efficiency less than half of that of the 3aCFP/3aYFP group, indicating that 3a protein itself forms dimers and tetramers that are prevented by M6 mutation (Fig. 3*D*). These data suggest that 3a proteins form homopolymerization that may be critical for their function.

3a Protein Is Functionally Expressed in *Xenopus* Oocytes and Modulates Membrane Current. Based on 3a protein localization and the tetramerization analysis, we proposed that 3a protein may function as an ion channel. To assess whether 3a protein is a potential ion channel, *Xenopus* oocytes were injected with complement RNA (cRNA) of 3a protein or its mutant (M6). This system is well established to test viral protein function as an ion channel (12). The 3a protein expression for both wild-type and M6 mutant was revealed on the oocyte cell membranes by anti-LH21 Ab and confocal microscopy (Fig. 4 *B* and *C*). Western blots of lysed oocytes injected with either 3a or M6 mutant 3a protein cRNAs showed similar patterns of protein expression (Fig. 4*D*). These results demonstrate that wild-type and M6 mutant 3a proteins are expressed on the cell membrane of injected *Xenopus* oocytes. This feature is essential for 3a protein functional analysis.

In preliminary experiments, several ions, such as proton, sodium, calcium, and potassium, were tested in oocytes (data not shown).

MICROBIOLOGY

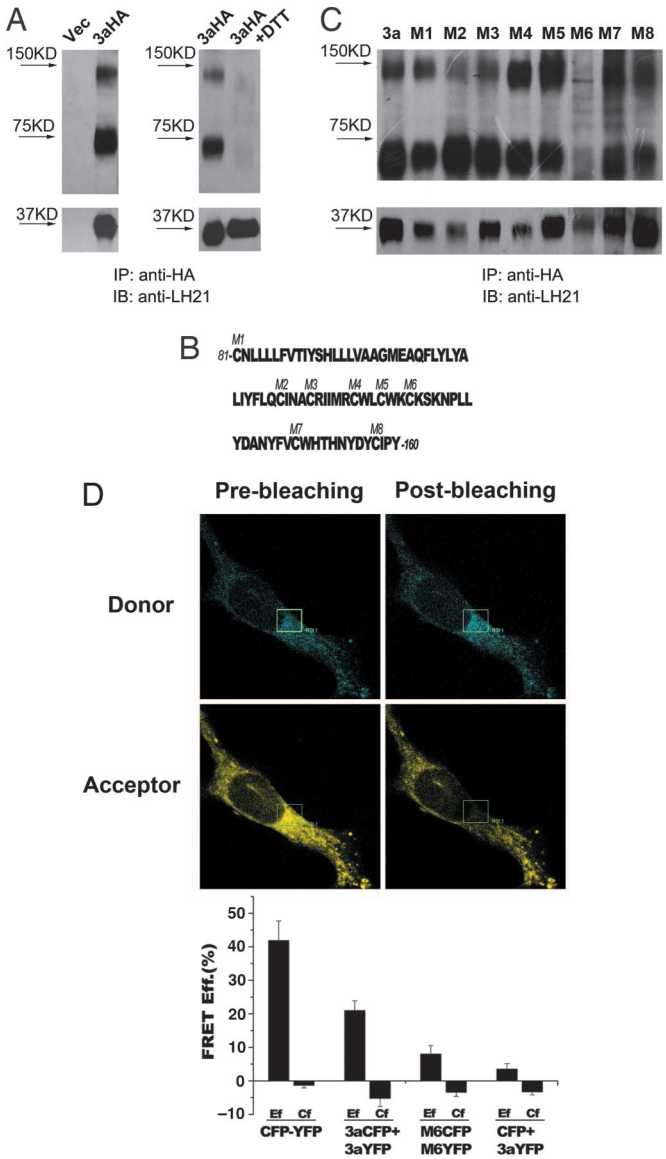

Fig. 3. The 3a protein forms homodimers and tetramers. (*A*) A complex by immunoprecipitation using anti-HA Ab was detected by anti-LH21 Ab. The control group of HEK293 cells was transfected only with vector (Vec), and the 3a group was transfected with 3a plasmid fused with HA tag (3aHA). DTT was used to disrupt the disulfide bond formation. (*B*) Eight point mutants on different cysteines in the 3a protein are marked in the map (amino acid residues 81–160). (*C*) Eight mutants of 3a protein, M1–M8, were tested by immunoprecipitation. (*D*) FRET (pseudocolor) analysis of the homooligomeric 3a protein in HeLa cells. Emission spectra of 3aCFP and 3aYFP before and after photobleaching are presented. The averaged FRET efficiency of YFP–CFP fusion protein (as a positive control), 3aCFP and 3aYFP, M6CFP and M6YFP, as well as CFP and 3aYFP (as a negative control) of 10 cells each was calculated. Ef, FRET efficiency of a photobleaching region; Cf, same calculations for a nonbleaching region ($n = 10$).

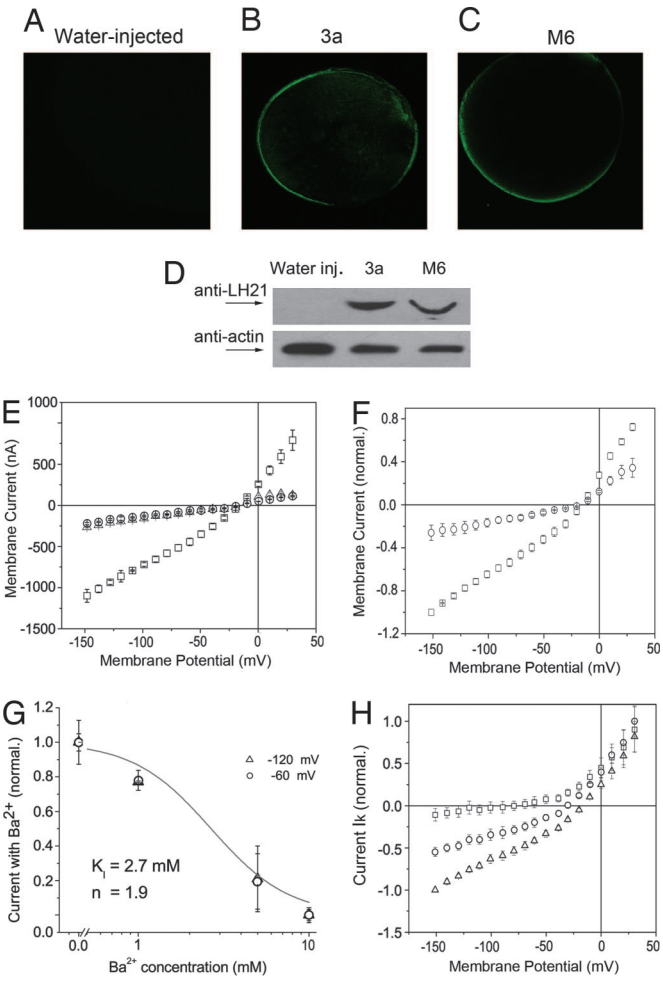

Fig. 4. The 3a protein forms an ion channel in *Xenopus* oocytes. Water-injected (*A*), 3a-cRNA-injected (*B*), and M6-cRNA-injected (*C*) oocytes were immunolabeled with anti-LH21 and monitored by confocal microscopy. (*D*) The oocytes were also lysed, and 3a protein was analyzed by Western blot. (*E*) Voltage dependencies of steady-state currents in control oocytes (open circles) and in oocytes with expressed 3a (open squares) or M6 protein (open triangles) in potassium (100 mM) buffer. (*F*) Inhibition of the 3a-mediated potassium-sensitive current by barium (open squares, 100 mM potassium buffer; open circles, in the presence of 10 mM $BaCl_2$). (*G*) Dependence of the barium-sensitive current at −120 and −60 mV on barium concentration. The solid line represents a fit of Eq. **1**. (*H*) Voltage dependencies of potassium current in bath solutions with different potassium concentrations (100 mM, open triangles; 50 mM, open circles; 10 mM, open squares). $I_K = I_{Total} - I_{Ba}$; I_K, the barium-inhibited potassium current; I_{Total}, the total current; I_{Ba}, current with the presence of 10 mM barium. For concentrations <100 mM, potassium was substituted with tetramethylammonium. All data represent averages of at least three oocytes + SEM.

We observed that oocytes expressing 3a protein at their membrane surface led to a dramatic increase of membrane current over the entire potential range in 100 mM potassium solution (Fig. 4*E*). Therefore, in this study we focused only on testing whether 3a protein could serve as a potassium ion channel.

Because the M6 mutant cannot form homotetramers, which may be crucial for channel formation, we compared membrane current in wild-type and M6 mutant of 3a protein cRNA-injected oocytes. Expression of M6 mutant 3a protein, in contrast to expression of the native 3a protein, did not result in an increase of membrane current when extracellular potassium concentration was kept at 100 mM; the current was similar to that of noninjected oocytes (Fig. 4*E*). To investigate whether the 3a protein-mediated conductance has characteristics of an ion channel, a variety of typical potassium channel blockers, such as tetraethylammonium, cesium, barium, and the antiviral drug Amanatadine, were tested. None of them, except for barium, affected the extra current registered after expression of 3a protein (data not shown). The 3a-mediated potassium-sensitive current could be completely blocked by 10 mM barium in the bath solution (Fig. 4*F*). The inhibition of the current by different barium concentrations was plotted for two different potentials (−120 and −60 mV) showing voltage-independent inhibition (Fig. 4*G*). A fit of

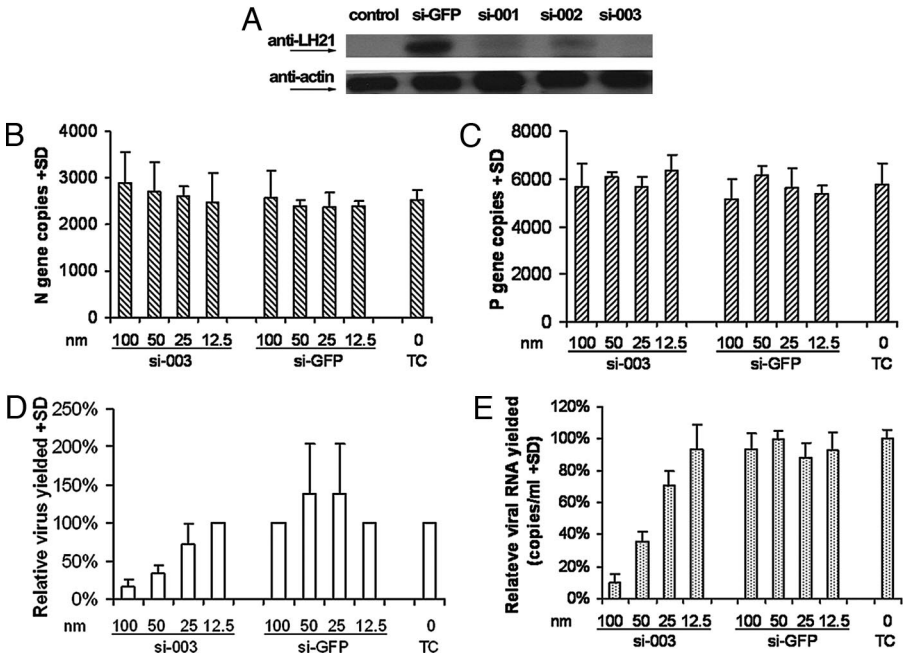

Fig. 5. SARS-CoV release is inhibited in 3a protein-suppressed FRhK-4 cells. (*A*) Three siRNAs targeting the 3a gene were cotransfected with the 3a expression plasmid 3aHA into FRhK-4 cells, and the suppressing effect of these siRNAs on 3a protein expression was detected by Western blot assay. Different concentrations (100, 50, 25, and 12.5 nM) of the most effective siRNA (si-003) and an unrelated siRNA (si-GFP, as negative control) were transfected into FRhK-4 cells. After incubation for 6 h, cells were infected with 100 $TCID_{50}$ of SARS-CoV. Seventy-two hours after infection, intracellular SARS-CoV was measured by real-time quantitative RT-PCR in triplicate to determine copies of viral N gene (*B*) and P gene (*C*). The results were expressed as viral RNA copies per copy of β-actin, and the SDs are given. The relative virus yield in cell supernatant was titrated by $TCID_{50}$ (*D*), and its genome was quantified by real-time RT-PCR in triplicate (*E*). The results from siRNA-pretreated cultures were compared with those from control transfectant (TC, defined as 100%). SDs are indicated. The virus release into the cell culture of the si-003-pretreated group was significantly reduced as compared with the si-GFP-pretreated group ($P < 0.01$).

$$I = \frac{K_I^n}{K_I^n + [Ba^{2+}]^n} \quad [1]$$

yielded a K_I value of 2.7 mM with a Hill coefficient of $n = 1.9$. Fig. 4*H* shows current–voltage dependencies of the barium-inhibited current component ($I_K = I_{Total} - I_{Ba}$) for different potassium concentrations. The current increase paralleled the increase in potassium concentration, and the reversal potential was shifted considerably in the negative direction with decreasing potassium concentration, suggesting that this current is mediated by potassium-permeable channels. Whether this channel is potassium-selective still needs further investigation. Taken together, these data suggest that 3a protein behaves like an ion channel that is permeable for potassium.

SARS-CoV Release Is Inhibited in 3a Protein-Suppressed FRhK-4 Cells. To date, in general, ion channels for viral proteins control virus entry or release, such as M2 protein of influenza virus and Vpu protein of HIV-1 (13, 14). Based on this notion, the regulation of 3a protein on SARS-CoV entry or release was investigated by an siRNA approach. Initially, three siRNA candidates with sequences complementary to ORF-3a regions were synthesized, and their capacity to suppress 3a protein expression in FRhK-4 cells was evaluated by Western blot analysis. The data showed that all three siRNA candidates suppressed the 3a protein expression at a concentration of 100 nM, but si-003 appeared the most effective (Fig. 5*A*). Thus, si-003 was selected for the following experiments.

When 3a protein expression was blocked by the siRNA (si-003), the cytopathic effect appeared 3 days after infection and was similar to that observed in SARS-CoV-infected cells without siRNA pretreatment (data not shown). The numbers of copies of intracellular viral N gene (Fig. 5*B*) and P gene (Fig. 5*C*) were similar between siRNA-pretreated and nonpretreated infected cells; it is likely that siRNA did not affect virus infection and viral RNA replication.

However, titers ($TCID_{50}$) and genomic RNA (real-time quantitative RT-PCR) of virus released into culture media were reduced to 10% at 100 nM, 35% at 50 nM, and 70% at 25 nM in si-003-pretreated cell cultures, as compared with cultures pretreated with the transfectant alone (Fig. 5 *D* and *E*). The results suggest that the viral 3a protein function may contribute to the release of the virus from infected cells. However, we cannot exclude that alternatively, or additionally, a reduced expression of 3a protein may hamper packaging of virus particles or affect localization and assembly at a later viral replication stage.

Discussion

SARS-CoV is a newly identified coronavirus in humans that leads to a dangerous acute inflammation and is more lethal than other human coronaviruses (1–3). Beyond the four basic structural proteins, S, M, E, and N proteins, viral replicase, and protease, other structural and nonstructural proteins have not been fully studied. Identification of these viral proteins and understanding of their functions will help in development of effective drug candidates for SARS therapy.

The existence of 3a protein in both purified virus particles and virus-infected cell lysates has been reported (4, 6). Few studies have shown that the 3a protein may be involved in cell apoptosis (15, 16) and may be released from virus-infected cells or 3a protein-transfected cells (17). In the present study we have demonstrated the antibody response to 3a protein in SARS patients and confirmed the expression of 3a protein in SARS-CoV-infected cells. We have also analyzed its localization and structure on the cell membrane and found for the first time that 3a protein forms homodimers and homotetramers in transfected and possibly in infected cells. Localization of 3a protein on the membrane of virus-infected cells may be transient as a large part of it. 3a protein may be either incorporated into the virion (6) or released in the extracellular compartment in an unidentified form (17). Thus, in our experiments 3a could be identified and characterized only when it was expressed individually in transfected cells. However, processing of 3a protein in SARS-CoV-infected cells deserves further studies using pulse–chase experiments unaffordable in our biosafety level 3 laboratory.

The tetrameric pattern is a very common feature of a protein involved in ion channel formation (18). Therefore, we tested whether the 3a protein could mediate channel-like activity by a two-electrode voltage clamp in *Xenopus* oocytes. Indeed, 3a protein expression resulted in a membrane current that was sensitive to potassium ions, suggesting the formation of a potassium-permeable channel-like structure. This idea was supported by the inhibitory

effect on 3a-mediated current by barium ions. To what extent this ion channel is potassium-selective still needs to be investigated.

The formation of a pore structure in virus-infected cell membrane makes the cell more permeable, an important factor for the SARS-CoV lifespan. Our experiments demonstrated that SARS-CoV release is effectively inhibited by using si-003 to suppress 3a protein expression in the virus-infected FRhK-4 cells. Although we cannot exclude the possibility that the decrease of virus release after suppressing 3a protein expression may be due to insufficient structural 3a protein necessary for virus packaging or affecting viral replication at the later stage by suppressing other viral protein expression, location, and assembly, our results, taken together, indicate that the 3a protein modulates virus release.

Until now, only few ion channel proteins for viruses have been identified. The Kcv protein of *Paramecium bursaria* chlorella virus forms a potassium channel (12), whereas the M2 protein of influenza virus forms a proton channel (19). Two other viral proteins, Vpu and Vpr of HIV, have also been reported to have channel activity (20, 21). The functions of these ion channels vary among one another. The Kcv is associated with virus replication (12), and M2 is reported to assist in influenza A virus infection (22).

Our findings are to some extent similar to those of Vpu protein in HIV-1. Vpu protein forms a channel selective for monovalent cations when reconstituted in lipid bilayers, and expression in *Xenopus* oocytes leads to an increase in membrane conductance (20, 23). Vpu protein is not required for HIV-1 egression, but it can make the virus release more efficient (24, 25). It was also reported that Vpu could interact with the human TWIK-related acid-sensitive potassium channel (TASK) and inhibit its activity, suggesting that the conductance caused or modified by Vpu may help the HIV virus to be released from infected cells more efficiently (26). However, the detailed mechanism of how these ion channels modulate the virus release is still a puzzle.

It was thought that M and E proteins are the major proteins for coronavirus assembly and budding (27, 28) and that 3a protein may not be essential for the virus life cycle, because some coronaviruses do not show an intact expression pattern for this locus (4). But our data demonstrated that 3a can definitely influence the virus release, although the mechanism should be further investigated.

The present study highlights the 3a protein function of the highly pathogenic SARS-CoV. A deeper understanding of the ion channel activity of 3a protein will help to elucidate its role in viral lifespan and pathogenesis. It is hoped that further study of modulation of virus release mediated by 3a protein will provide new keys to the understanding of the pathogenesis of SARS or other coronavirus infections.

Materials and Methods

Plasmids. The coding sequence of SARS-CoV (GenBank accession no. AY279354) 3a protein was subcloned into the mammalian expression plasmid pBudCE4.1 (Invitrogen, Carlsbad, CA) for transient transfection and protein expression. Protein 3a cDNA was a generous gift from Ruifu Yang (Institute of Microbiology and Epidemiology, Academy of Military Medical Sciences, Beijing, China). Then, at the C terminus of the 3a protein sequence, a HA tag was added for immunoprecipitation, whereas two additional tags, CFP and YFP, were used for FRET. Eight point mutated 3a plasmids were constructed by two-step PCR. Each of the eight cysteines in 3a protein was mutated to alanine by using eight pairs of specific primers containing the point mutation.

Antibodies. The polyclonal anti-3a Ab (anti-LH21) was obtained from the Antibody Research Center (Shanghai Institute of Biochemistry and Cellular Biology, Chinese Academy of Sciences). This Ab was custom-produced against a synthetic peptide derived from the N terminus of SARS-CoV 3a protein (amino acids 4–24, FMRFFTLGSITAQPVKIDNAS). Monoclonal Ab anti-HA was purchased from Santa Cruz Biotechnology (Santa Cruz, CA).

ELISA. Peptide (LH21) derived from the N terminus of the 3a protein was used for detection of specific IgG against the 3a protein in SARS patient sera. The peptide used as the detecting antigen was conjugated with BSA and coated on 96-well microplates at a concentration of 5 μg/ml. 3a protein-specific IgG was assayed in sera of 13 SARS patients (confirmed by clinical symptoms and ELISA determination of anti-spike protein-specific antibodies; Institute of Microbiology and Epidemiology, Academy of Military Medical Sciences, Beijing, China). Thirteen healthy subjects were selected as negative controls. The serum samples were diluted to 1:100 and incubated for 2 h, and the secondary Ab (HRP-conjugated anti-human IgG, BD Biosciences, San Jose, CA) was added and incubated for another hour. The OD_{450} value was measured in a Microplate Reader (Thermo, Waltham, MA).

Cell Culture, Transfection, and Virus Infection. HEK293, HeLa, and FRhK-4 cells (from American Type Culture Collection, Manassas, VA) were cultured in DMEM containing 10% FBS (Gibco, Carlsbad, CA) at 37°C in a CO_2 incubator. Lipofectamine 2000 (Invitrogen) was used for transient transfection following the manufacturer's protocols. For SARS-CoV infection, FRhK-4 cells were inoculated with virus (GZ 50 strain) at a multiplicity of infection (moi) of 5 for 1 h in medium without FBS. The cells were washed with medium and cultured with complete medium for 24 h or longer. All preocedures were performed in a biosfety level 3 laboratory.

Immunohistochemistry and Confocal Microscopy. SARS-CoV-infected FRhK-4 cells on pretreated glass slides were fixed with 4% paraformaldehyde and then immunolabeled with polyclonal Ab anti-LH21 at a 1:500 dilution for 1 h. The cells were then incubated with FITC-conjugated secondary Ab (BD Biosciences) at a 1:100 dilution for 30 min. FRhK-4 cells transfected with HA-tagged 3a plasmid for 48 h were first fixed with 5% paraformaldehyde, then either permeabilized by 70% ethanol or not permeabilized. Finally, the cells were immunolabeled with anti-LH21 (1:500 dilution) or anti-HA (1:100 dilution). Localization of the 3a-labeled protein was studied by using a TCS SP2 confocal microscope (Leica Microsystems, Wetzlar, Germany).

Immunoprecipitation and Western Blot. Expression of the 3a protein in HEK293 cells was studied 24–36 h after transient transfection. The cells were lysed in 10× RIPA lysis buffer [0.5 M Tris·HCl, pH 7.4/1.5 M NaCl/2.5% deoxycholic acid/10% Nonidet P-40/10 mM EDTA] at 4°C for 30 min. Cell lysates were centrifuged at 12,000 × *g* for 15 min, and the supernatant was preincubated with anti-HA monoclonal Ab at 4°C for 1–2 h. Then, protein A/G (Santa Cruz Biotechnology) beads were added to the cell lysates and incubated at 4°C overnight. Beads were washed five times with RIPA buffer. Finally, the complex was eluted by using 2× SDS buffer and subjected to SDS/PAGE (29). Proteins were transferred to a nitrocellulose membrane, and protein 3a was detected by anti-LH21 at a 1:3,000 dilution. The secondary Ab HRP-conjugated anti-rabbit IgG was used at a 1:4,000 dilution. FRhK-4 cells were infected with SARS-CoV for 24 h and collected as described previously (4). Infected cells were lysed with a solution containing 40 mM Tris (pH 8.3) and 0.5% Nonidet P-40 at 22°C for 5 min. The virus lysate was centrifuged at 10,000 × *g* for 5 min, and the supernatant was collected and boiled for 5 min. The infected cell lysate (5 μl) was subjected to SDS/PAGE and treated as described above.

FRET. Forty-eight hours after transfection with recombinant 3a expression plasmids, HeLa cells were fixed with 4% paraformaldehyde and mounted on a slide. Cell observation and FRET efficiency calculation were performed by using a TCS SP2 confocal microscope and its analytical software for FRET bleaching. Emission spectra from cells expressing 3aCFP and 3aYFP were obtained

by using 405-nm laser lines. Selected areas near the cell membrane of 3aYFP were photobleached with 514-nm laser lines. FRET was resolved as an increase in 3aCFP (donor) signal after photobleaching of 3aYFP (acceptor). FRET efficiency was calculated as $[1 - (\text{CFP } I_{\text{prebleach}}/\text{CFP } I_{\text{postbleach}})] \times 100\%$.

Similar calculations were performed in a nonbleached region to obtain the parameter Cf. Cf. represents an internal control value.

Expression of the 3a Protein in Oocytes. The protein 3a cDNA was cloned into pNWM vector (a gift from Jian Fei, Shanghai Institute of Biological Sciences, Chinese Academy of Sciences) downstream of a SP6 promoter used for mRNA *in vitro* transcription. PCR products were digested with restriction enzymes SalI and BglII and ligated into the plasmid. Protein 3a cRNA was synthesized by the mMESSAGE mMACHINE high-yield capped RNA transcription SP6 kit (Ambion, Austin, TX) and injected into *Xenopus laevis* oocytes (10 ng per oocyte). Oocytes were obtained and prepared according to standard methods (12). Forty-eight hours after injection, the oocytes were used for electrophysiology and immunofluorescence or lysed for immunoblotting analysis.

Electrophysiology. Two-electrode voltage clamp is a reliable method for testing the electrogenic activity of a membrane protein. It allows measurement of the current flow at different defined membrane potentials. Two-electrode voltage clamp equipment (Turbo TEC 10, NPI Electronic, Tamm, Germany) was used to record the currents from the plasma membrane of *Xenopus* oocytes with or without expressed 3a protein. The standard voltage-clamp protocol consisted of rectangular voltage steps from −150 to +30 mV in 10-mV increments applied from a holding voltage of −60 mV. Microelectrodes were filled with 3 M KCl and had a resistance of 0.5–1 MΩ. The oocytes were superfused at room temperature (≈22°C) with standard bath solution [ORi containing 90 mM NaCl, 2 mM KCl, 2 mM $CaCl_2$, and 5 mM Hepes (pH 7.4)]. The experimental solutions had a composition of 100 mM KCl, 1.8 mM $CaCl_2$, 1 mM $MgCl_2$, and 5 mM Hepes (pH 7.4). Solutions containing different concentrations of potassium (for concentrations <100 mM, potassium was substituted with tetramethylammonium) were used. The other components in the solution were the same as above.

Design of siRNA Targeting the 3a Gene and Suppressing 3a Expression. Three siRNAs targeting the 3a gene were designed according to criteria previously described (30) and were chemically synthesized by Ribobio (GuangZhou, China). These three siRNA candidates (si-001 sequence, TGCATCAACGCATGTAGAA; si-002 sequence, AGATACAATTGTCGTTACT; si-003 sequence, CAGCTTGAGTCTACACAAA) were cotransfected at 100 nM concentration with 3a plasmid (0.5 μg) into FRhK-4 cells in a 24-well plate. An unrelated siRNA (si-GFP) was included in the experiment as negative control. After culture for 24 h, the effects of siRNAs in suppressing 3a expression were determined by Western blot assay using anti-LH21 as described above. The most effective siRNA in suppressing 3a expression was selected for the SARS-CoV infection assay.

Functional Analysis of siRNA Targeting the 3a Gene in SARS-CoV-Infected Cells. The most effective siRNA (si-003) for 3a protein expression at different concentrations (100, 50, 25, and 12.5 nM) and an unrelated siRNA control (si-GFP) were transfected into FRhK-4 cells. After incubation at 37°C for 6 h, 100 $TCID_{50}$ of SARS-CoV was inoculated into the cell cultures. Seventy-two hours after infection, the SARS-CoV-induced cytopathic effect was evaluated in transfected and infected cells. Virus yields ($TCID_{50}$) in cell supernatants were titrated, and copies of viral RNA in cell supernatants and in infected cells were also determined by real-time quantitative RT-PCR in triplicate as described (31–33). The relative virus yield in cell supernatant was calculated based on the values obtained from cultures pretreated with siRNAs and transfectant alone (the value from transfectant pretreated cultures was set at 100%).

We thank Miss Yan Zhang (Nanjing University, Nanjing, China), Dr. Yu Li (National Institute of Allergy and Infectious Diseases, National Institutes of Health, Bethesda, MD), and Prof. Hailing Zhang (Hebei Medical University, Hebei, China) for technical support and Dr. Sheri Skinner and Profs. Guoping Zhou and Zhihong Hu for reviewing the manuscript and for helpful comments. This work was supported by Technology Commission of Shanghai Municipality Grants 04DZ14902 and 04DZ19108, National Key Basic Research Program of China Grant 2001CB510006, National Natural Science Foundations of China Grants 30421005 and 30530700, Outstanding Young Scientist Fund of the National Natural Science Foundation of China Grants 30228016 and 30325018, Sino-German Center on SARS Project Grant GZ238 (202/11), and an E-Institutes of Shanghai Universities Immunology Division grant.

1. Drosten, C., Gunther, S., Preiser, W., van der Werf, S., Brodt, H. R., Becker, S., Rabenau, H., Panning, M., Kolesnikova, L., Fouchier, R. A., *et al*. (2003) *N. Engl. J. Med.* **348,** 1967–1976.
2. Ksiazek, T. G., Erdman, D., Goldsmith, C. S., Zaki, S. R., Peret, T., Emery, S., Tong, S., Urbani, C., Comer, J. A., Lim, W., *et al*. (2003) *N. Engl. J. Med.* **348,** 1953–1966.
3. Marra, M. A., Jones, S. J., Astell, C. R., Holt, R. A., Brooks-Wilson, A., Butterfield, Y. S., Khattra, J., Asano, J. K., Barber, S. A., Chan, S. Y., *et al*. (2003) *Science* **300,** 1399–1404.
4. Zeng, R., Yang, R. F., Shi, M. D., Jiang, M. R., Xie, Y. H., Ruan, H. Q., Jiang, X. S., Shi, L., Zhou, H., Zhang, L., *et al*. (2004) *J. Mol. Biol.* **341,** 271–279.
5. Yu, C. J., Chen, Y. C., Hsiao, C. H., Kuo, T. C., Chang, S. C., Lu, C. Y., Wei, W. C., Lee, C. H., Huang, L. M., Chang, M. F., *et al*. (2004) *FEBS Lett.* **565,** 111–116.
6. Ito, N., Mossel, E. C., Narayanan, K., Popov, V. L., Huang, C., Inoue, T., Peters, C. J. & Makino, S. (2005) *J. Virol.* **79,** 3182–3186.
7. Yuan, X., Li, J., Shan, Y., Yang, Z., Zhao, Z., Chen, B., Yao, Z., Dong, B., Wang, S., Chen, J., *et al*. (2005) *Virus Res.* **109,** 191–202.
8. Shen, S., Lin, P. S., Chao, Y. C., Zhang, A., Yang, X., Lim, S. G., Hong, W. & Tan, Y. J. (2005) *Biochem. Biophys. Res. Commun.* **330,** 286–292.
9. Tan, Y. J., Teng, E., Shen, S., Tan, T. H. P., Goh, P. Y., Fielding, B. C., Ooi, E. E., Tan, H. C., Lim, S. G. & Hong, W. (2004) *J. Virol.* **78,** 6723–6734.
10. Kerschensteiner, D., Soto, F. & Stocker, M. (2005) *Proc. Natl. Acad. Sci. USA* **102,** 6160–6165.
11. Kotevic, I., Kirschner, K. M., Porzig, H. & Baltensperger, K. (2005) *Cell. Signalling* **17,** 869–880.
12. Plugge, B., Gazzarrini, S., Nelson, M., Cerana, R., Van Etten, J. L., Derst, C., DiFrancesco, D., Moroni, A. & Thiel, G. (2000) *Science* **287,** 1641–1644.
13. Kelly, M. L., Cook, J. A., Brown-Augsburger, P., Heinz, B. A., Smith, M. C. & Pinto, L. H. (2003) *FEBS Lett.* **552,** 61–67.
14. Montal, M. (2003) *FEBS Lett.* **552,** 47–53.
15. Tan, Y. J., Fielding, B. C., Goh, P. Y., Shen, S., Tan, T. H., Lim, S. G. & Hong, W. (2004) *J. Virol.* **78,** 14043–14047.
16. Law, P. T., Wong, C. H., Au, T. C., Chuck, C. P., Kong, S. K., Chan, P. K., To, K. F., Lo, A. W., Chan, J. Y., Suen, Y. K., *et al*. (2005) *J. Gen. Virol.* **86,** 1921–1930.
17. Huang, C., Narayanan, K., Ito, N., Peters, C. J. & Makino, S. (2006) *J. Virol.* **80,** 210–217.
18. Shi, N., Ye, S., Alam, A., Chen, L. & Jiang, Y. (2006) *Nature* **440,** 570–574.
19. Pinto, L. H., Holsinger, L. J. & Lamb, R. A. (1992) *Cell* **69,** 517–528.
20. Ewart, G. D., Sutherland, T., Gage, P. W. & Cox, G. B. (1996) *J. Virol.* **70,** 7108–7115.
21. Piller, S. C., Ewart, G. D., Premkumar, A., Cox, G. B. & Gage, P. W. (1996) *Proc. Natl. Acad. Sci. USA* **93,** 111–115.
22. Ciampor, F., Cmarko, D., Cmarkova, J. & Zavodska, E. (1995) *Acta Virol.* **39,** 171–181.
23. Schubert, U., Ferrer-Montiel, A. V., Oblatt-Montal, M., Henklein, P., Strebel, K. & Montal, M. (1996) *FEBS Lett.* **398,** 12–18.
24. Gottlinger, H. G., Dorfman, T., Sodroski, J. G. & Haseltine, W. A. (1991) *Proc. Natl. Acad. Sci. USA* **88,** 3195–3199.
25. Gottlinger, H. G., Dorfman, T., Cohen, E. A. & Haseltine, W. A. (1993) *Proc. Natl. Acad. Sci. USA* **90,** 7381–7385.
26. Hsu, K., Seharaseyon, J., Dong, P., Bour, S. & Marban, E. (2004) *Mol. Cell* **14,** 259–267.
27. Corse, E. & Machamer, C. E. (2000) *J. Virol.* **74,** 4319–4326.
28. Maeda, J., Maeda, A. & Makino, S. (1999) *Virology* **263,** 265–272.
29. Sugure, R. J. & Hay, A. J. (1990) *Virology* **180,** 617–624.
30. Reynolds, A., Leake, D., Boese, Q., Scaringe, S., Marshall, W. S. & Khvorova, A. (2004) *Nat. Biotechnol.* **22,** 326–330.
31. He, M. L., Zheng, B., Peng, Y., Peiris, J. S., Poon, L. L., Yuen, K. Y., Lin, M. C., Kung, H. F. & Guan, Y. (2003) *J. Am. Med. Assoc.* **290,** 2665–2666.
32. Zheng, B. J., Guan, Y., Tang, Q., Du, C., Xie, F. Y., He, M. L., Chan, K. W., Wong, K. L., Lader, E., Woodle, M. C., *et al*. (2004) *Antiviral Ther.* **9,** 365–374.
33. Zheng, B. J., Guan, Y., Hez, M. L., Sun, H., Du, L., Zheng, Y., Wong, K. L., Chen, H., Chen, Y., Lu, L., *et al*. (2005) *Antiviral Ther.* **10,** 393–403.